ACS Photonics

Article

pubs.acs.org/journal/apchd5

Direct Band Gap Germanium Microdisks Obtained with Silicon Nitride Stressor Layers

Moustafa El Kurdi,[†] Mathias Prost,[†] Abdelhamid Ghrib,[†] Sébastien Sauvage,[†] Xavier Checoury,[†] Grégoire Beaudoin,[‡] Isabelle Sagnes,[‡] Gennaro Picardi,[§] Razvigor Ossikovski,[§] and Philippe Boucaud*[,†]

[†]Institut d'Electronique Fondamentale, CNRS, Univ. Paris-Sud, Université Paris-Saclay, Bâtiment 220, Rue André Ampère, F-91405 Orsay, France

[‡]Laboratoire de Photonique et de Nanostructures, CNRS-UPR20, Route de Nozay, F-91460 Marcoussis, France

[§]Laboratoire de Physique des Interfaces et des Couches Minces, CNRS, Ecole polytechnique, Université Paris-Saclay, F-91128 Palaiseau, France

S *Supporting Information*

ABSTRACT: Germanium is an ideal candidate to achieve a monolithically integrated laser source on silicon. Unfortunately bulk germanium is an indirect band gap semiconductor. Here, we demonstrate that a thick germanium layer can be transformed from an indirect into a direct band gap semiconductor by using silicon nitride stressor layers. We achieve 1.75% (1.67%) biaxial tensile strain in 6 (9) μm diameter microdisks as measured from photoluminescence. The modeling of the photoluminescence amplitude vs temperature indicates that the zone-center Γ valley has the same energy as the L valley for a 9 μm diameter strained microdisk and is even less for the 6 μm diameter microdisk, thus demonstrating that a direct band gap is indeed obtained. We deduce that the crossover in germanium from indirect to direct gap occurs for a 1.67% ± 0.05% biaxial strain at room temperature, the value of this parameter varying between 1.55% and 2% in the literature.

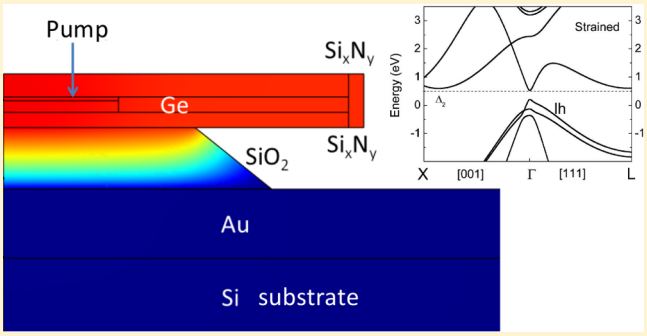

KEYWORDS: *silicon photonics, microdisk resonators, photoluminescence, germanium, infrared source, direct band gap semiconductor, strain engineering*

A direct band gap semiconductor is expected to exhibit an efficient radiative recombination and the possibility to obtain optical gain with reasonable injected carrier densities. For these reasons, significant efforts have been devoted to engineer the band structure of germanium, which is, in its bulk form, an indirect band gap semiconductor. The transition from indirect to direct band structure can be obtained by applying tensile strain since the position in energy of the different bands varies differentially as a function of the strain present in the layers.[1] One expects that a direct band gap germanium could be used as an efficient room-temperature monolithically integrated optical source for silicon photonics.

In the literature, several approaches have been reported to obtain a direct band gap germanium. Up to 2.33% biaxial tensile strain has been demonstrated with 10 nm thick Ge films grown on InGaAs buffer layers with a larger lattice constant as compared to germanium.[2] Biaxial tensile strain up to 1.78% was obtained in mechanically deformed nanomembranes.[3,4] Direct band gap was achieved by micropatterning germanium on silicon and transferring uniaxial strains up to 5.7%.[5] We note that direct band gap germanium can also be obtained by alloying with tin.[6−9] Another approach to transfer a significant tensile strain in germanium is the use of external stressor layers such as silicon nitride.[10−14] Biaxial tensile strain up to 1.5% was demonstrated in ref 15 using an all-around stressor layer approach, i.e., a stressor layer below and above the germanium film.

In this Letter, we show that biaxial tensile strain up to 1.75% can be transferred in germanium microdisks using silicon nitride stressor layers. The tensile strain is monitored by Raman as well as room-temperature and variable-temperature photoluminescence measurements. The temperature-dependent modeling of photoluminescence shows that the energy of the zone-center Γ valley is the same as that of the L valley for a 9 μm diameter microdisk, thus confirming the direct band gap nature of the 190 nm thick Ge. In the literature, the crossover from indirect to direct band gap has been predicted for tensile strain values mainly varying between 1.55% and 2% at room temperature.[4,16−21] The variation of this key figure of merit mainly stems from the uncertainty on the deformation potentials to be considered. Our measurements indicate that

Received: November 9, 2015
Published: February 3, 2016

DOI: 10.1021/acsphotonics.5b00632
ACS Photonics 2016, 3, 443−448

the crossover is rather around 1.67% ± 0.05%, and we provide a set of deformation potential parameters that allow a good fit of the photoluminescence spectra.

RESULTS

The whole fabrication process with the all-around silicon nitride layer is described in the Materials and Methods section. Figure 1a shows, as an example, a scanning electron microscopy image of a 9 μm diameter microdisk before the deposition of the upper silicon nitride layer. Figure 1b and c show the Raman spectra recorded in backscattering geometry around the Ge−Ge vibration mode for a strained 6 μm diameter microdisk (b) and a strained 9 μm diameter microdisk (c). In both cases, the Raman spectra are compared with that of a reference germanium film grown on GaAs. This reference sample corresponds to a blanket Ge on GaAs film grown in the same conditions as for the processed sample. In the latter case, a small 0.07% compressive stress, as measured by X-ray diffraction, is present in the Ge film. A significant shift for the Raman peak of 8.4 cm^{-1} is observed for the 6 μm strained microdisk. This shift corresponds to a 1.93% biaxial tensile strain if we use the relationship $\Delta\omega = -b\varepsilon$ with b = 415 cm^{-1} and ε the in-plane strain component.[22] An even higher value (2.08%) is obtained if we consider a b coefficient value of 390 cm^{-1}.[12] There is thus an uncertainty of around 0.15% on the strain state as deduced from the Raman signature of the Ge−Ge vibration mode. For the 9 μm strained microdisk, the biaxial strain is around 1.6−1.7%. As compared to previous reports on all-around strained microdisks, the transferred strain is higher because of a thinner germanium thickness (190 nm instead of 500 nm in ref 15). The increase of strain transfer by reducing the Ge thickness is confirmed by finite-element modeling, as shown in the Supporting Information (Supplementary S1). The penetration depth of the laser used for Raman spectroscopy is around 20 nm in Ge. Consequently, the Raman measurements provide information on the strain state at the top surface of the Ge film. For optoelectronic emission devices, it is more relevant to estimate the strain from the photoluminescence spectrum since it is a signature of the stress transfer in a larger volume where optical recombinations take place. Figure 2a shows the room-temperature photoluminescence of the 6 μm diameter microdisk. The emission is peaked around 2240 nm, as compared to 1545 nm for the direct band gap emission in unstrained germanium. This large shift is a direct consequence of the strong dependence of the zone-center Γ valley vs applied strain along with the hole energy splitting with strain. At this level of strain and for a moderate carrier injection, the photoluminescence is dominated by the direct recombination between the Γ valley and the light hole band. Moreover, the energy splitting between light hole and heavy hole recombination is sufficiently large to allow identifying unambiguously the light hole recombination even if one does not exactly know the collection efficiency between TE and TM polarizations. The

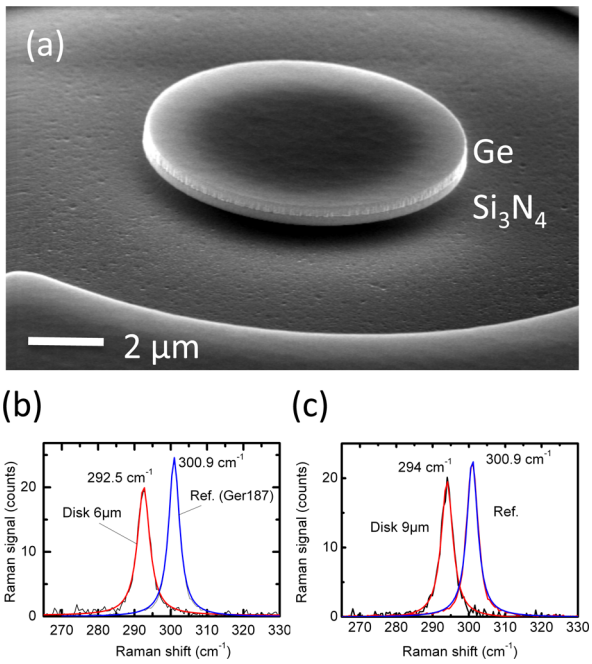

Figure 1. (a) Scanning electron microscopy image of a 9 μm diameter microdisk before the deposition of the second silicon nitride layer. The buried silicon oxide pedestal is not directly observed but appears with the darkened contrast at the microdisk center. One can observe the bottom silicon nitride layer and the active Ge layer. (b) Raman spectrum for an all-around 6 μm diameter strained microdisk. The Raman resonance is compared to a reference blanket Ge on GaAs grown in the same conditions as for the processed sample. (c) Same Raman measurement for a 9 μm diameter all-around strained microdisk.

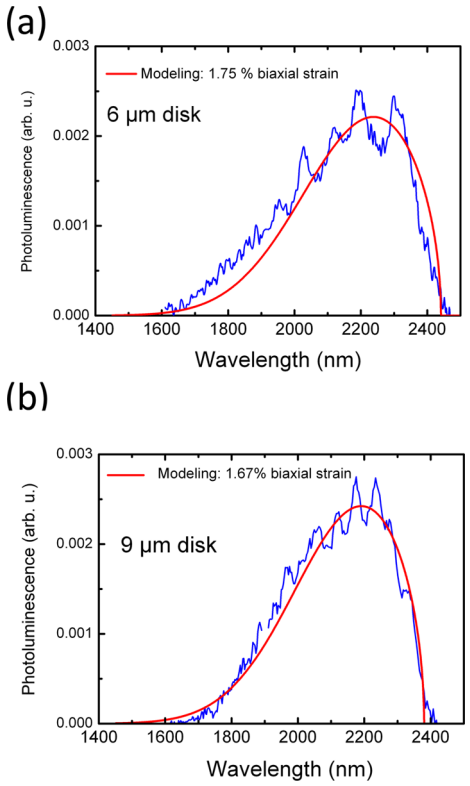

Figure 2. (a) Room-temperature photoluminescence of an all-around 6 μm diameter strained microdisk. The photoluminescence is measured with a single-channel extended-wavelength InGaAs detector and collected with a Cassegrain objective. The spectrum is corrected from the optical system response. The red full line is a modeling of the emission taking into account a 1.75% biaxial tensile strain. (b) Room-temperature photoluminescence of a 9 μm diameter microdisk. The red full line is a modeling of the emission taking into account a 1.67% biaxial tensile strain.

DOI: 10.1021/acsphotonics.5b00632
ACS Photonics 2016, 3, 443−448

spectrum is modulated by a series of low-quality-factor resonances that correspond to Fabry−Perot modes along the disk diameter.[13] We have superimposed on this emission spectrum the modeling of the photoluminescence. This modeling accounts for both light hole (LH) and heavy hole (HH) recombinations and their different dipole matrix elements for both TE and TM polarizations, but the recombination can be well fit by considering only transitions between Γ valley and the light hole band. The modeling also accounts for a 17 meV band gap narrowing due to the n-doping of Ge.[23,24] This value is the one that gives the best agreement for the photoluminescence fit of the reference sample also used in Raman measurements. The best fit in Figure 2a is obtained by considering an average 1.75% biaxial tensile strain present in the microdisk. This value is slightly smaller than the one obtained by Raman, as a consequence of the larger volume probed by the carrier optical recombination. The key feature is that we have achieved significantly higher strain values as compared to previous demonstration with this all-around stressor layer approach (1.5%).[15] These types of microdisks are thus likely to exhibit a direct band gap. In order to confirm this hypothesis, we have performed temperature-dependent photoluminescence measurements. The experiments were performed on a 9 μm diameter microdisk. This disk has a larger pedestal and better thermal management as compared to the 6 μm diameter microdisk. It can thus reach low temperatures under moderate continuous wave optical pumping. Meanwhile, with a better thermal dissipation, one avoids the enhanced emission that results for high-temperature glowing gray-body emission.[25]

Figure 2b shows the room-temperature photoluminescence of a 9 μm diameter microdisk. The transferred strain is slightly smaller as compared to the previous case, and the best fit of the emission spectrum is obtained with 1.67% biaxial tensile strain consistent with the strain field deduced by Raman measurements. This result illustrates the robustness of the process that leads to high strain values on a full series of microdisks. Figure 3 shows the photoluminescence spectra as a function of temperature for the 9 μm diameter microdisk. The measurements are recorded with a multichannel photodetector, and the emission is collected with a microscope objective. In this figure, the indicated temperature is the disk temperature that accounts for the energy deposited by the optical pumping. The effective temperature of the microdisk is calculated by finite elements by considering the temperature-dependent thermal conductivity of silicon oxide. For a 2.6 mW optical pumping, the lowest temperature that could be achieved is around 120 K (see supplementary S2 for more details). The key factor that limits the disk cooling is the pedestal diameter. A variation of ±1 μm leads to a variation of (−15,+20) K at low temperature. The variation is stronger when the disk pedestal diameter is reduced. The effect is less marked at elevated temperature. We observe a significant increase of the direct band gap photoluminescence amplitude as the temperature is decreased. Similar temperature-dependent measurements were performed on reference unstrained Ge samples. In this case, we observe an increase of the indirect band gap recombination by a factor of 30 when the temperature is lowered, whereas the direct band gap recombination vanishes at low temperature (see supplementary S3). The modeling of the temperature dependence of the indirect band gap emission allows one to deduce the temperature dependence of the photoinduced carrier density. This dependence can be accounted for through Shockley−Read−Hall recombinations (see supplementary S3).[26,27] There is an increase by a factor of 6.5 of the photoinduced carrier density from room temperature to low temperature. We emphasize that, for strained germanium, the emission in Figure 3 is dominated by the direct band gap recombination and not by the indirect band gap recombination involving the L valley. Indeed, the room-temperature amplitude of the strained microdisk is much larger as compared to the indirect band gap recombination of the blanket structure (factor of about 100).

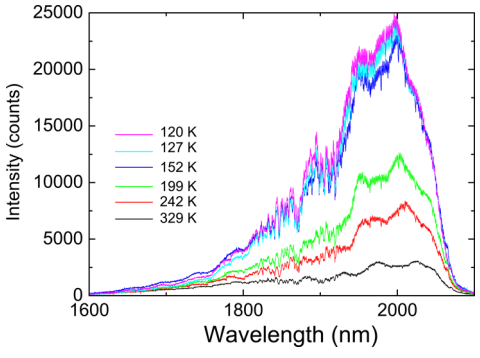

Figure 3. Photoluminescence of an all-around 9 μm diameter strained microdisk at different temperatures. The photoluminescence is collected with a multichannel linear array InGaAs detector through a microscope objective. The effective microdisk temperatures in the presence of the optical pumping are indicated on the graph. The optical pump density at 632.8 nm incident on the sample is 3.7×10^4 W cm^{-2}.

DISCUSSION

The peak amplitude of the emission is reported as a function of temperature in Figure 4. The values are normalized to the values at room temperature. To extract the data, the following procedure has been used. Figure 2 shows that the peak maximum for spectra in Figure 3 is beyond the cutoff of the detector at elevated temperature. We have thus applied a correction factor, deduced from the modeling, to retrieve the

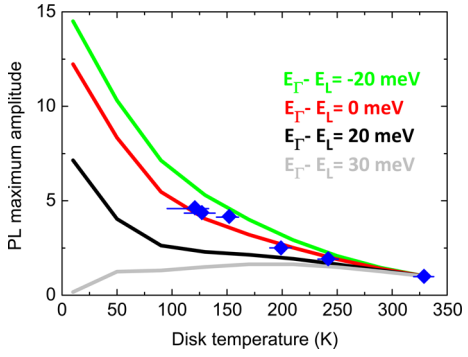

Figure 4. Maximum amplitude of the photoluminescence of a 9 μm diameter strained microdisk as a function of temperature (diamonds). The amplitude has been set to 1 for room-temperature measurement. A correction factor is considered to account for the detector cutoff. The full lines correspond to the amplitude predicted by modeling with indirect and direct valleys. The variable is the energy difference between the Γ valley and the L valley (from bottom to top: +30 meV, +20 meV: indirect band gap semiconductor; 0, −20 meV: direct band gap semiconductor). The horizontal error bar on the temperature corresponds to a pedestal diameter variation of ±1 μm.

DOI: 10.1021/acsphotonics.5b00632
ACS Photonics 2016, 3, 443−448

photoluminescence maximum when it occurs beyond the cutoff (see Figure 2 with a measurement done with a broadband detector). This correction factor is given by the ratio between the PL at 2 μm and the one at the maximum. The indicated temperatures are those calculated in the microdisk core by taking into account the energy deposited by the optical pumping. These values are also correlated to the peak maximum in energy following Varshni's law.[28] We have superimposed on this figure four modelings with different energy differences between the zone-center Γ valley and the L valley: +30 and +20, i.e., an indirect band gap semiconductor, 0 meV, i.e., the crossover from indirect to direct band gap, −20 meV, corresponding to a direct band gap configuration. The modeling accounts for the photoinduced carrier density vs temperature as measured from the unstrained blanket reference structures as described in Supplementary S3. The data are obtained with unstrained material but for the same Ge thickness and Ge/SiN interfaces as for the processed material. They provide a value for the energy difference of the trap states with the Fermi level. The modeling also accounts for the energy difference between Γ and L that varies by around 9 meV as a function of temperature.[28] The 10^{19} cm^{-3} n-type doping of the germanium layer is considered. Note that this feature limits the relative increase of the emission between room temperature and low temperature. The photoinduced carrier density is around 6×10^{17} cm^{-3} at room temperature. With an indirect band gap semiconductor characterized by a 20 meV Γ−L splitting, one would expect only a small increase of the direct band gap emission at low temperature. It should even decrease for larger splittings (30 meV and above). Figure 4 clearly shows that the best fit of the data for a 9 μm diameter microdisk is obtained for a Γ−L splitting equal to 0 meV, i.e., at the crossover from the indirect and direct band gap. We have obtained the same conclusion by considering the amplitude of the emission at 1940 nm, i.e., without tracking the PL maximum and applying correction factors. Similar temperature-dependent measurements could not be performed on 6 μm diameter microdisks since the very small pedestal size prevents getting to low temperature. However, as Raman measurements indicate that the strain state is larger than for the 6 μm diameter microdisk (1.9% instead of 1.6%), we deduce that the Γ valley lies below the L valley for these microdisks.

We have thus two independent estimates of the strain state through photoluminescence measurements. The modeling of the spectral shape (Figure 2) indicates a 1.67% biaxial tensile strain, while the modeling of the amplitude vs temperature indicates a 0 meV energy difference between Γ and L valleys. The main interest of the modeling in Figure 4 is that it only depends on the energy difference between the conduction bands, whereas Raman or modeling of photoluminescence in Figure 2 depends on the strain state and on the presupposed energy variation vs strain. Both measurements are consistent if one considers that the crossover between the indirect and direct band structure occurs around 1.67% biaxial tensile strain at room temperature. As mentioned above, there is a large spread for this crossover value in the literature from 1.55% to 2% and above. The sets of photoluminescence experiments on tensile-strained microdisks provide thus an indirect measurement of this parameter that is rather in the low range of the various estimates. This value agrees with those reported in refs 17, 19, and 20. The uncertainty on the Γ−L splitting measured from Figure 4 is around ±5 meV. It corresponds to an uncertainty of ±0.05% on the strain field to reach the crossover, i.e., 1.67 ± 0.05%. We obtain a very satisfying fit of the photoluminescence data by considering the following parameters that describe the variation of the band edges vs strain using standard deformation potential theory:[4,18,19,29] $a_c^{\Gamma} - a_v = -8.97$ eV, $b_{\Gamma^{5+}} = -1.88$ eV, in agreement with the values reported in ref 30. Without considering the band gap narrowing, the fit would be obtained with the values $a_c^{\Gamma} - a_v = -9.75$ eV, $b_{\Gamma^{5+}} = -1.88$ eV. We note that there is a large spread of values for these deformation potentials[30] that leads to an uncertainty on the biaxial strain field on the order of 0.1%. Here these values are used for highly strained Ge films where the variation of the band gap energy is very significant. Beyond the demonstration of direct band gap germanium with silicon nitride stressor layers, these measurements provide an experimental estimate of the indirect to direct band gap crossover, a very important parameter for the development of efficient germanium optical sources for silicon photonics.

In conclusion, we have fabricated tensile-strained germanium microdisks using an all-around silicon nitride encapsulation. The microdisks were characterized by Raman and temperature-dependent photoluminescence spectroscopy. Both the spectral shape and the amplitude of the photoluminescence were modeled. The modeling indicates that the Γ−L splitting was near 0 meV for 9 μm diameter microdisks. It demonstrated that direct band gap germanium can be obtained using all-around silicon nitride stressor layers. A higher strain state and consequently a Γ valley below the L valley were obtained for 6 μm diameter microdisks. These measurements have also emphasized the importance of thermal management in such microdisks. The size of the pedestal limits the lower temperature that can be reached under continuous wave (CW) optical excitation. This feature needs to be taken into account for laser operation of such microdisks under pulsed or CW optical pumping.

MATERIALS AND METHODS

Sample Fabrication. The investigated germanium samples were grown by metal−organic chemical vapor deposition on a GaAs substrate.[31] They consist of a 190 nm thick germanium layer deposited on an AlGaAs etch stop layer on GaAs. Isobutyl-germane was used as germanium precursor. An AsH_3 flow is maintained during growth and provides an *in situ* n-type doping of the Ge film around 10^{19} cm^{-3}. The stress is transferred following the all-around processing steps described in ref 15: a compressively strained 230 nm thick silicon nitride layer is first deposited by plasma-enhanced chemical vapor deposition. It is followed by a 850 nm thick SiO_2 layer. The whole structure is bonded on a silicon substrate using Au−Au bonding. The GaAs substrate is then removed by wet etching, and microdisks with various diameters are patterned by e-beam lithography. Figure 1a shows a scanning electron microscopy image of the fabricated microdisks at this step. A second nitride layer (300 nm thick) is then deposited on the top and at the edges of the structure. The germanium layer is thus fully embedded in silicon nitride stressor layers, thus justifying the all-around denomination. The symmetry of the disk leads to a transfer of a biaxial strain, a key feature to achieve direct band gap Ge. Moreover, the microdisks provide a resonant cavity since they can support whispering gallery modes. The reference sample (Ger187) used for the Raman measurements is a 700 nm thick Ge layer grown in the same conditions by metal−organic chemical vapor deposition on a GaAs substrate.

DOI: 10.1021/acsphotonics.5b00632
ACS Photonics 2016, 3, 443−448

Experimental Setup. The photoluminescence measurements were performed either with a single-channel extended InGaAs photodetector with a cutoff wavelength of 2.4 μm or a linear array multichannel InGaAs detector. We have used either achromatic Cassegrain mirrors or high numerical aperture microscope objectives for collection. The photoluminescence is excited with a CW He−Ne laser that emits at 632.8 nm. The Raman spectra were obtained in backscattering geometry with a 532 nm excitation light.

■ ASSOCIATED CONTENT

Supporting Information

The Supporting Information is available free of charge on the ACS Publications website at DOI: 10.1021/acsphotonics.5b00632.

Details on the modeling of the strain field and disk temperature and on the carrier density dependence with temperature (PDF)

■ AUTHOR INFORMATION

Corresponding Author

*E-mail: philippe.boucaud@ief.u-psud.fr.

Notes

The authors declare no competing financial interest.

■ ACKNOWLEDGMENTS

This work was supported by Agence Nationale de la Recherche under GRAAL convention (ANR Blanc call 2011 BS03 00401) and by "Triangle de la Physique" under Gerlas convention. This work is also partially supported by a public grant overseen by the French National Research Agency (ANR) as part of the "Investissements d'Avenir" program (Labex NanoSaclay, reference: ANR-10-LABX-0035). We acknowledge support from the RENATECH network. We thank A. Elbaz for his contribution to temperature modeling.

■ REFERENCES

(1) Liu, J.; Sun, X.; Pan, D.; Wang, X.; Kimerling, L. C.; Koch, T. L.; Michel, J. Tensile-strained, n-type Ge as a gain medium for monolithic laser integration on Si. *Opt. Express* **2007**, *15*, 11272−11277.

(2) Huo, Y.; Lin, H.; Chen, R.; Makarova, M.; Rong, Y.; Li, M.; Kamins, T. I.; Vuckovic, J.; Harris, J. S. Strong enhancement of direct transition photoluminescence with highly tensile-strained Ge grown by molecular beam epitaxy. *Appl. Phys. Lett.* **2011**, *98*, 011111.

(3) Sanchez-Perez, J. R.; Boztug, C.; Chen, F.; Sudradjat, F. F.; Paskiewicz, D. M.; Jacobson, R.; Lagally, M. G.; Paiella, R. Direct-bandgap light-emitting germanium in tensilely strained nanomembranes. *Proc. Natl. Acad. Sci. U. S. A.* **2011**, *108*, 18893−18898.

(4) Boztug, C.; Sanchez-Perez, J. R.; Cavallo, F.; Lagally, M. G.; Paiella, R. Strained-Germanium Nanostructures for Infrared Photonics. *ACS Nano* **2014**, *8*, 3136−3151.

(5) Sukhdeo, D. S.; Nam, D.; Kang, J.-H.; Brongersma, M. L.; Saraswat, K. C. Direct bandgap germanium-on-silicon inferred from 5.7% uniaxial tensile strain. *Photonics Res.* **2014**, *2*, A8−A13.

(6) D'Costa, V. R.; Cook, C. S.; Birdwell, A. G.; Littler, C. L.; Canonico, M.; Zollner, S.; Kouvetakis, J.; Menéndez, J. Optical critical points of thin-film Ge_{1-y} Sn_y alloys: A comparative $Ge_{1-y}Sn_yGe_{1-x}Si_x$ study. *Phys. Rev. B: Condens. Matter Mater. Phys.* **2006**, *73*, 125207.

(7) Gallagher, J. D.; Xu, C.; Jiang, L.; Kouvetakis, J.; Menéndez, J. Fundamental band gap and direct-indirect crossover in $Ge_{1-x-y}Si_xSn_y$ alloys. *Appl. Phys. Lett.* **2013**, *103*, 202104.

(8) Gupta, S.; Magyari-Kope, B.; Nishi, Y.; Saraswat, K. C. Achieving direct band gap in germanium through integration of Sn alloying and external strain. *J. Appl. Phys.* **2013**, *113*, 073707−7.

(9) Wirths, S.; Geiger, R.; von den Driesch, N.; Mussler, G.; Stoica, T.; Mantl, S.; Ikonic, Z.; Luysberg, M.; Chiussi, S.; Hartmann, J.-M.; Sigg, H.; Faist, J.; Buca, D.; Grutzmacher, D. Lasing in direct-bandgap GeSn alloy grown on Si. *Nat. Photonics* **2015**, *9*, 88−92.

(10) de Kersauson, M.; El Kurdi, M.; David, S.; Checoury, X.; Fishman, G.; Sauvage, S.; Jakomin, R.; Beaudoin, G.; Sagnes, I.; Boucaud, P. Optical gain in single tensile-strained germanium photonic wire. *Opt. Express* **2011**, *19*, 17925−17934.

(11) Nam, D.; Sukhdeo, D.; Cheng, S.-L.; Roy, A.; Huang, K. C.-Y.; Brongersma, M.; Nishi, Y.; Saraswat, K. Electroluminescence from strained germanium membranes and implications for an efficient Si-compatible laser. *Appl. Phys. Lett.* **2012**, *100*, 131112.

(12) Capellini, G.; Kozlowski, G.; Yamamoto, Y.; Lisker, M.; Wenger, C.; Niu, G.; Zaumseil, P.; Tillack, B.; Ghrib, A.; de Kersauson, M.; El Kurdi, M.; Boucaud, P.; Schroeder, T. Strain analysis in SiN/Ge microstructures obtained via Si-complementary metal oxide semiconductor compatible approach. *J. Appl. Phys.* **2013**, *113*, 013513.

(13) Ghrib, A.; El Kurdi, M.; de Kersauson, M.; Prost, M.; Sauvage, S.; Checoury, X.; Beaudoin, G.; Sagnes, I.; Boucaud, P. Tensile-strained germanium microdisks. *Appl. Phys. Lett.* **2013**, *102*, 221112.

(14) Millar, R.; Gallacher, K.; Samarelli, A.; Frigerio, J.; Chrastina, D.; Isella, G.; Dieing, T.; Paul, D. Extending the emission wavelength of Ge nanopillars to 2.25% using silicon nitride stressors. *Opt. Express* **2015**, *23*, 18193−18202.

(15) Ghrib, A.; El Kurdi, M.; Prost, M.; Sauvage, S.; Checoury, X.; Beaudoin, G.; Chaigneau, M.; Ossikovski, R.; Sagnes, I.; Boucaud, P. All-Around SiN Stressor for High and Homogeneous Tensile Strain in Germanium Microdisk Cavities. *Adv. Opt. Mater.* **2015**, *3*, 353−358.

(16) Soref, R. A.; Friedman, L. Direct-gap Ge/GeSn/Si and GeSn/Ge/Si heterostructures. *Superlattices Microstruct.* **1993**, *14*, 189−193.

(17) Fischetti, M. V.; Laux, S. E. Band structure, deformation potentials, and carrier mobility in strained Si, Ge, and SiGe alloys. *J. Appl. Phys.* **1996**, *80*, 2234−2252.

(18) El Kurdi, M.; Fishman, G.; Sauvage, S.; Boucaud, P. Band structure and optical gain of tensile-strained germanium based on a 30 band $\mathbf{k}\cdot\mathbf{p}$ formalism. *J. Appl. Phys.* **2010**, *107*, 013710.

(19) Virgilio, M.; Manganelli, C. L.; Grosso, G.; Pizzi, G.; Capellini, G. Radiative recombination and optical gain spectra in biaxially strained n-type germanium. *Phys. Rev. B: Condens. Matter Mater. Phys.* **2013**, *87*, 235313.

(20) Kao, K.-H.; Verhulst, A. S.; Van de Put, M.; Vandenberghe, W. G.; Soree, B.; Magnus, W.; De Meyer, K. Tensile strained Ge tunnel field-effect transistors: $\mathbf{k}\cdot\mathbf{p}$ material modeling and numerical device simulation. *J. Appl. Phys.* **2014**, *115*, 044505.

(21) Wen, H.; Bellotti, E. Rigorous theory of the radiative and gain characteristics of silicon and germanium lasing media. *Phys. Rev. B: Condens. Matter Mater. Phys.* **2015**, *91*, 035307.

(22) Boucaud, P.; El Kurdi, M.; Ghrib, A.; Prost, M.; de Kersauson, M.; Sauvage, S.; Aniel, F.; Checoury, X.; Beaudoin, G.; Largeau, L.; Sagnes, I.; Ndong, G.; Chaigneau, M.; Ossikovski, R. Recent advances in germanium emission. *Photonics Res.* **2013**, *1*, 102−109.

(23) Oehme, M.; Gollhofer, M.; Widmann, D.; Schmid, M.; Kaschel, M.; Kasper, E.; Schulze, J. Direct bandgap narrowing in Ge LEDs on Si substrates. *Opt. Express* **2013**, *21*, 2206−2211.

(24) Camacho-Aguilera, R.; Han, Z.; Cai, Y.; Kimerling, L. C.; Michel, J. Direct band gap narrowing in highly doped Ge. *Appl. Phys. Lett.* **2013**, *102*, 152106.

(25) Boucaud, P.; El Kurdi, M.; Sauvage, S.; de Kersauson, M.; Ghrib, A.; Checoury, X. Light emission from strained germanium. *Nat. Photonics* **2013**, *7*, 162−162.

(26) Shockley, W.; Read, W. T. Statistics of the Recombinations of Holes and Electrons. *Phys. Rev.* **1952**, *87*, 835−842.

(27) Schubert, E. F. *Light-Emitting Diodes*; Cambridge University Press, 2006; p 434.

(28) Varshni, Y. Temperature dependence of the energy gap in semiconductors. *Physica* **1967**, *34*, 149−154.

(29) Cardona, M.; Pollak, F. H. Energy-Band Structure of Germanium and Silicon: The k·p Method. *Phys. Rev.* **1966**, *142*, 530−543.

DOI: 10.1021/acsphotonics.5b00632
ACS Photonics 2016, 3, 443−448

(30) Liu, J.; Cannon, D. D.; Wada, K.; Ishikawa, Y.; Danielson, D. T.; Jongthammanurak, S.; Michel, J.; Kimerling, L. C. Deformation potential constants of biaxially tensile stressed Ge epitaxial films on Si(100). *Phys. Rev. B: Condens. Matter Mater. Phys.* **2004**, *70*, 155309.
(31) de Kersauson, M.; Jakomin, R.; El Kurdi, M.; Beaudoin, G.; Zerounian, N.; Aniel, F.; Sauvage, S.; Sagnes, I.; Boucaud, P. Direct and indirect band gap room temperature electroluminescence of Ge diodes. *J. Appl. Phys.* **2010**, *108*, 023105.

DOI: 10.1021/acsphotonics.5b00632
ACS Photonics 2016, 3, 443−448